The plastically crystalline phase of NaOH, NaOD, KOH and KOD

1995 J. Phys.: Condens. Matter 7 7453

(http://iopscience.iop.org/0953-8984/7/38/005)

J. Phys.: Condens. Matter 7 (1995) 7453–7474. Printed in the UK

The plastically crystalline phase of NaOH, NaOD, KOH and KOD

U Schotte†‡, K D Schotte§, H-J Bleif†, M Kabs†‖ and H Dachs†

† Berlin Neutron Scattering Centre (Neutron Scattering Group), Hahn Meitner Institut, Glienickerstrasse 100, D-14109 Berlin, Germany

‡ Mineralogisches Institut, Universität Kiel, Germany

§ Theoretische Physik, Freie Universität, Berlin, Germany

Received 16 May 1995

Abstract. The high-temperature cubic phases of sodium hydroxide and potassium hydroxide have been investigated using x-ray, elastic and inelastic neutron scattering from single crystals. As a special feature of these experiments the crystals had to be kept at temperatures of around 550 K as grown from melt, since they are destroyed when passing through the structural phase transition.

In these compounds the OH or OD groups are known to undergo rapid reorientational motions.

The x-ray diffraction results are characterized by a rapid decrease in the Bragg intensities with increasing diffraction angle and diffuse rods passing through the Bragg reflections.

By neutron diffraction, about 20 symmetrically non-equivalent reflections have been observed. Different means of analysis will be presented; one obtains the probability distribution of H^+ or D^+ around oxygen, and the OH distance. This is of interest in the context of possible H bonding and proton conductivity.

The disorder of H or D gives rise to diffuse scattering of neutrons as an approximately spherical halo around the origin in Q-space. The orientations of OH groups at different sites being correlated cannot be excluded from the experimental findings; a 2D correlation model, however, does not predict a dramatic narrowing of this halo.

Inelastic scattering yielded rather ill-defined phonon groups in constant-Q scans. In particular, the shear modes showed strong overdamping. The observed features can be explained by treating the OH groups as elastic dipoles coupled to the lattice distortions, with the dynamics of a relaxator, and by extending conventional soft-mode theory to allow for the mixing of several softened modes. The softened modes also explain the diffuse rods in x-ray photographs.

1. Introduction

NaOH, NaOD, KOH and KOD are known to have the NaCl structure at high temperatures. The OH or OD molecules obtain cubic site symmetry by fast reorientational motions (Bleif and Dachs 1982, Kabs 1982, Mach *et al* 1987). Because of these motions the cubic phase can be called plastically crystalline (Sherwood 1979). As a mesomorphic phase between the crystalline and the liquid state it deserves special interest. More recently El'kin (1990) showed polycrystalline samples to be proton conductors.

The OH dynamics in NaOH have been investigated by incoherent neutron scattering of a powder sample. The results were interpreted as rotational jumps of the proton on the

‖ Present address: Heraeus Holding GmbH, Hanau, Germany.

0953-8984/95/387453+22$19.50

corners of a cube around the oxygen with a 'residence time' of about 10^{-12} s (Smit *et al* 1979). Further investigations of the structure and dynamics require the use of single crystals, the preparation and handling of which proved to be quite a challenge. The crystals when cooled through the cubic–monoclinic phase transition near 566 K for NaOH and NaOD and 513 K for KOH and KOD will not become single crystals again on heating. Therefore they have to be kept in a range of 30 K for NaOH and NaOD and of 120 K for KOH and KOD above their respective transition temperatures. Table 1 reviews data on the structures and phase transition temperatures.

Table 1. *Phase transition temperatures of* NaOH, NaOD, KOH *and* KOD.

NaOH[a]	NaOD	KOH	KOD[b]
From 592 K	593 K	678 K	646 K
$Fm3m$	$Fm3m$	$Fm3m$	$Fm3m$
At 566 K to	561 K	517 K[c]	523 K
$P21/m$	$P21/m$	$P21/m$[d]	$P21/m$
At 514 K to	500 K	227.5 K[e]	(466 K)[f]
$Cmcm$	$Cmcm$ at	$P21/n$[g]	$P21/m$
< 6 K	153.2 K[h]		251 K
	$P21/n$[i]		$P21/n$
	< 6 K		< 16 K

[a] Bleif and Dachs (1982).
[b] Mach *et al* (1987).
[c] Maurice (1968).
[d] Ibers *et al* (1969).
[e] Stull *et al* (1970).
[f] Thermal anomaly observed by Mach *et al* (1987).
[g] Bastow *et al* (1986b).
[h] White and Moore (1986).
[i] Bastow *et al* (1986a).

For the investigation, x-ray and neutron diffraction and spectroscopy were available. In the following we describe experimental and theoretical work on the structure determination, namely the hydrogen probability distribution, diffuse x-ray scattering, disorder scattering of neutrons seen as a diffuse halo and finally phonon softening and damping behaviour caused by the coupling between OH reorientations and lattice distortions.

The theory for the structural dynamics has been developed before in the context of explaining inelastic data for the co-operative Jahn–Teller compound $CsCuCl_3$ (Schotte *et al* 1989) and applied to the inelastic data for KOD in an earlier publication (Schotte *et al* 1992) (hereafter referred to as I). Preliminary results on the structural work are being published in the context of the applicability of the maximum-entropy method (Schotte *et al* 1995).

2. Experimental details

For the preparation of KOH and NaOH samples, commercially available pellets were used. They contain water and Na_2CO_3 as main impurities. For the influence of these impurities on the phase transition temperatures and the specific heat, see Bleif and Dachs (1982) and references therein.

NaOD was prepared by dissolving Na_2O in D_2O and removing the excess D_2O by heating the solution in vacuum using crucibles of sintered Al_2O_3. KOD was prepared by letting metallic K react with D_2O vapour in a nitrogen atmosphere. The single crystals were grown, by a modified Bridgeman method, in a thin-walled hermetically sealed Al tube which could be directly mounted on the neutron diffractometer. In order to check the quality of the crystal during growth the Laue diffraction pattern was monitored using an x-ray image converter system. Whenever more than one crystal had developed, the growing procedure was started all over again. About one out of 20 trials was successful.

For the structure determination, crystals with a diameter of 4 mm and a length of 10 mm have been used on four-circle diffractometers operating with neutrons of wavelengths 1.035 and 1.182 Å. Rotating-crystal x-ray photographs have been taken with Mo Kα radiation.

The crystals used for phonon spectroscopy on the IN2 spectrometer at the ILL (Grenoble) had a diameter of 12 mm and a length of 15 mm. The wavevectors used were $k = 2\pi/\lambda = 1.55$ and 2.66 Å^{-1}. The powder samples used were 12 mm in diameter and 30 mm in length. During the transport, for example from the HMI, Berlin, to the ILL, Grenoble, the single crystals were kept at a temperature of about 580 K using battery-operated temperature controllers.

3. Structure determination

The determination of the structure consists essentially in finding the probability density distribution (to be called density for short) of the protons (or deuterons). For each sample a total number of 200–350 reflections were observed by neutron diffraction and reduced to 17–21 symmetrically independent structure factors. The list of structure factors for NaOH and NaOD is given in table 1, and that for KOH and KOD can be found in the paper on the maximum-entropy method (Schotte *et al* 1995). There the main results for KOH and KOD have also been reported but not the procedures which we now describe in detail for the sodium compounds.

As a first approximation, split-atom models were fitted to the data with H or D distributed around O at distance R_H. In the rock-salt unit cell, O is taken at $(0, 0, 0)$ and Na at $(1/2, 1/2, 1/2)$. Some of H can now be assumed to be at distance R_H in $r_c = (1, 1, 1)R_H/\sqrt{3}$ and some in $r_e = (1, 1, 0)R_H/\sqrt{2}$ and all other equivalent positions. The structure factor is given by

$$F(Q) = F_{Na} + F_O + F_{H111} + F_{H110} \tag{1}$$

with $Q = (2\pi/a)(h, k, l)$ and

$$\begin{aligned} F_{Na} &= 4b_{Na}(-1)^h \exp(-\tfrac{1}{2}\langle u_{Na}^2\rangle Q^2) \\ F_O &= 4b_O \exp(-\tfrac{1}{2}\langle u_O^2\rangle Q^2) \\ F_{H111} &= b_{H111}\frac{A(r_c)}{6}\exp(-\tfrac{1}{2}\langle u_H^2\rangle Q^2) \\ F_{H110} &= b_{H110}\frac{A(r_e)}{4}\exp(-\tfrac{1}{2}\langle u_H^2\rangle Q^2) \end{aligned} \tag{2}$$

where (see international tables for Fm3m), for the general site $r = (x, y, z)$, A is given by

$$A(r) = 32\cos(hx)\cos(ky)\cos(lz) + \text{all permutations.} \tag{3}$$

The scattering lengths are given in table 2; for that of hydrogen, $b_H = 8b_{H111} + 12b_{H110}$ must hold. One can also add a contribution for the face centres at $(1, 0, 0)R_H$, etc, but this does not improve the fit.

Table 2. Structure factors from single-crystal neutron diffraction for NaOH and NaOD; data from Bleif (1978). The lattice constant is $a = 5.10$ Å and the space group Fm3m. The scattering lengths are $b_{Na} = 0.362 \times 10^{-12}$ cm, $b_O = 0.580 \times 10^{-12}$, $b_D = 0.667 \times 10^{-12}$ and $b_H = -0.374 \times 10^{-12}$. $F(000)$, although not measurable, is four times the sum of the scattering factors and consistent with the scaled experimental data.

hkl	F_{NaOH}	σ	F_{NaOD}	σ
000	2.272	—	6.346	—
111	0.370	0.017	1.940	0.020
200	2.090	0.102	3.190	0.035
220	1.840	0.105	1.970	0.022
311	0.900	0.033	0.444	0.017
222	1.430	0.063	1.410	0.017
400	1.160	0.037	0.574	0.016
331	0.490	0.019	0.444	0.022
420	0.740	0.027	0.557	0.020
422	0.480	0.020	0.520	0.019
511	0.330	0.015	0.255	0.037
333	0.240	0.014	0.410	0.024
440	0.230	0.019	0.344	0.039
531	0.190	0.020	0.223	0.051
600	0.140	0.019	0.272	0.030
442	0.180	0.035	0.292	0.043
620	0.130	0.052	0.187	0.060
533	—	—	0.167	0.082
622	—	—	0.146	0.080

To start with, the Debye–Waller (DW) factors are taken from the x-ray measurements; for NaOH, $\langle u_{Na}^2 \rangle = 0.18$ Å^2 and $\langle u_O^2 \rangle = 0.09$ Å^2; for NaOD, $\langle u_{Na}^2 \rangle = 0.15$ Å^2 and $\langle {}^2_{Na} \rangle = 0.08$ Å^2.

The fit parameters are determined by searching for the minimum value of

$$\chi^2 = \sum_\nu \frac{(F_{obs}(Q_\nu) - F_{calc}(Q_\nu))^2}{\sigma_\nu^2}.$$

One obtains an acceptable fit with all phase factors positive, which is mainly because O is the strongest scatterer and $F_O > 0$.

Already at this stage it has become clear that the hydrogen avoids the position closest to the alkali ion at the face centres.

The second step was to calculate a Fourier map and a difference Fourier map. For the latter the temperature factors were taken as above and slightly adjusted until nearly zero density was obtained at the sites of O and Na. The density is slightly higher in the 111 directions than in the 110 directions and much lower in the 100 directions; figure 1 gives a three-dimensional (3D) impression, for details see figure 2.

An analytical expression for the hydrogen density with reasonably few adjustable parameters can be obtained by expanding the scattering density in terms of symmetry-adapted spherical harmonics (Seymor and Pryor 1970, Press and Hüller 1973, Press 1973).

Instead on sites of cubic symmetry on a cube around O the hydrogen is taken to be distributed as

$$\rho_H(r) = \frac{\delta(r - R_H)}{4\pi R_H^2}(1 + c_{41} K_{41}(r)) \tag{4}$$

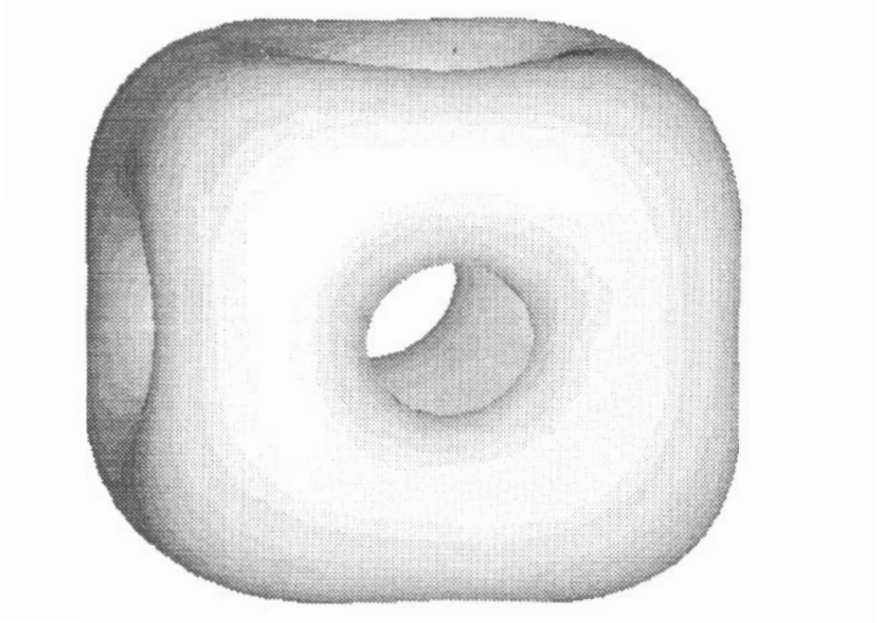

Figure 1. Probability density distribution of hydrogen in sodium hydroxide.

containing the cubic harmonic of fourth order:

$$K_{41}(r) = \frac{5\sqrt{21}}{4}\frac{x^4 + y^4 + z^4 - 3r^4/5}{r^4}$$

The c_{41} term describes the deviation from spherical symmetry. In principle, one can consider also terms of sixth and eighth order, but this is not worthwhile here since due to the large DW factors these terms turn out to involve tiny contributions which are not extractable from the structure data. For the structure factor, one needs the Fourier transform so that now

$$F(\boldsymbol{Q}) = F_O + F_{Na} + 4b_H\tilde{\rho}_H(\boldsymbol{Q})\exp(-\tfrac{1}{2}\langle u_H^2\rangle Q^2) \tag{5}$$

with

$$\tilde{\rho}_H(\boldsymbol{Q}) = j_0(\boldsymbol{Q}\cdot\boldsymbol{R}_H) + c_{41}K_{41}(\boldsymbol{Q})j_4(\boldsymbol{Q}\cdot\boldsymbol{R}_H) \tag{6}$$

where j_n are the spherical Bessel functions of order n:

$$\begin{aligned} j_0(x) &= \frac{\sin x}{x} \\ j_4(x) &= \frac{105\sin x - 105x\cos x - 45x^2\sin x + 10x^3\cos x + x^4\sin x}{x^5} \end{aligned} \tag{7}$$

If only $j_0(x)$ is taken into account, one has a spherical H density around the oxygen which is clearly not a good fit. The coefficient c_{41} has negative values which produces minima in the distribution in the ⟨100⟩ directions as expected. The sixth-order term gives no real improvement in the fits. Therefore one has five fit parameters: the OH radius, three DW factors and c_{41}. The parameters are given in table 3. Figure 3 shows the corresponding density contours of the hydrogen distribution in NaOD. The corresponding picture for NaOH is so similar that there is no need to show it. The parameters and plots for KOH and KOD are found in the paper on the maximum-entropy method referred to above. Again the pictures are very similar; the distribution in KOH and KOD is slightly more isotropic, and in KOH it is more isotropic than in KOD. Obviously it is reasonable to treat OH or OD as a rigid molecule with common DW factor.

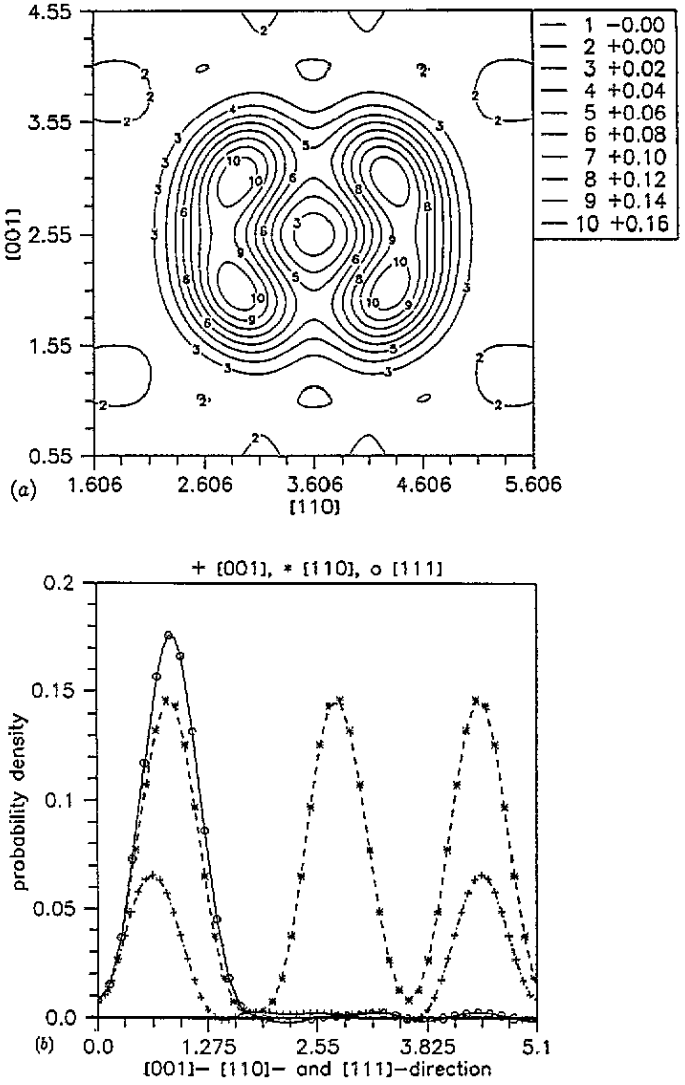

Figure 2. (*a*) Density distribution of D^+ in NaOD in the (110) plane from difference Fourier analysis. (*b*) Density profiles in several directions to show the anisotropy of the distribution quantitatively; note the difference in peak heights (left) for the [001] and [110] directions.

The hydrogen distribution of this model can be written in an analytical form. Convoluting (4) with the DW factor, one obtains

$$\rho_{HDW}(r) = \frac{1}{\sqrt{(2\pi\langle u_H^2\rangle)^3}} \exp\left(-\frac{r^2+R_H^2}{2\langle u_H^2\rangle}\right)\left[j_0\left(\frac{\mathrm{i}rR_H}{\langle u_H^2\rangle}\right) + c_{41}K_{41}(r)j_4\left(\frac{\mathrm{i}rR_H}{\langle u_H^2\rangle}\right)\right] \qquad (8)$$

which is similar to the structure factor, involving, however, Bessel functions of imaginary argument, i.e. cos and sin are replaced by their hyperbolic counterparts; equation (8) was used for plotting figures 1 and 3.

A remark has to be added regarding additional expansion terms of low order. Press *et al* (1979) suggested including correlations between orientation and centre-of-mass position

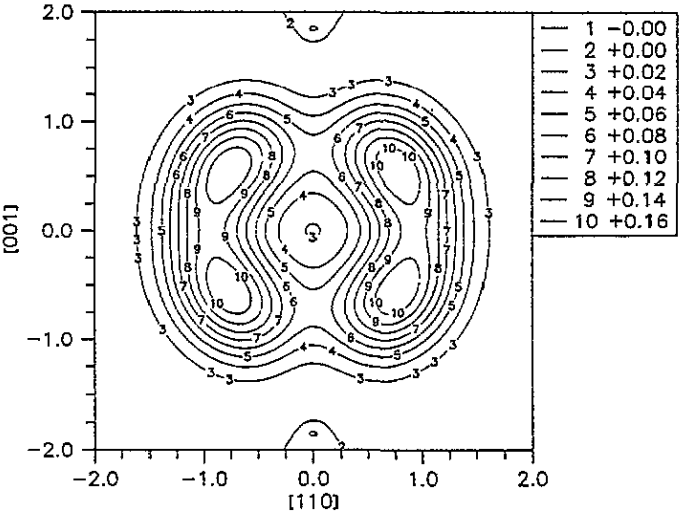

Figure 3. Density distribution of D^+ in NaOD in the (110) plane from the model fit with (8) and the parameters in table 3.

of a rigid molecule OH; assuming the position of H at r_H, one should take the angular average with respect to $R_H = r_H - R$, R being the instantaneous position of the molecular centre of mass given by $R = dR + R_0$, R_0 being the average position. If one Taylor expands with respect to dR, one obtains an additional fit parameter as the pre-factor of a term proportional to $\partial j_0(QR_H)/\partial R_H$ in (6). We found that this procedure did not give a better fit of the data or a significantly different value for R_H.

One sees that the OH difference is slightly greater than the OD distance; both stay below 1 Å so that H bonding to the next O ion as well as proton conduction in the pure stoichiometric crystal appear improbable.

No significant systematic difference between D and H compounds can be extracted from our data; only the temperature factors are larger for the H compounds and for the potassium compounds; there is a small difference in the anisotropies, namely KOH is more isotropic than KOD.

Table 3. Model fit parameters for the cubic structure of NaOH and NaOD.

	$R_{H/D}$	c_{41}	$\langle u_O^2 \rangle$	$\langle u_{H/D}^2 \rangle$	$\langle u_{Na}^2 \rangle$	χ^2	a (Å)
NaOH	0.97	−0.78	0.095	0.093	0.180	20.1	5.1
NaOD	0.93	−0.82	0.087	0.090	0.152	30.0	5.1

The temperature factors for the alkali ions are unusually large. This is probably the consequence of an evasive motion caused by the reorientations of the hydroxide group. Therefore translational–rotational coupling between these reorientations and lattice distortions are taken as the reason for the overdamping and other anomalous behaviour of the phonon groups, leading to the ill-defined phonon dispersions for the shear modes.

4. Thermodiffuse x-ray scattering

X-ray scattering of NaOH at 575 K was recorded photographically with Mo Kα radiation using a rotating-crystal camera. Two data sets have been recorded by rotating the crystal around the [001] and the [110] directions in steps of 5°. The photographs were scanned on a microdensitometer with a resolution of 0.1 mm × 0.1 mm; so it was possible to distinguish between the smooth diffuse scattering of the sample and the Debye–Scherrer rings from the aluminium crucible. After this correction the data were assigned reciprocal-lattice coordinates. Two layers are shown in figure 4. Essentially only K and O contribute to the x-ray scattering.

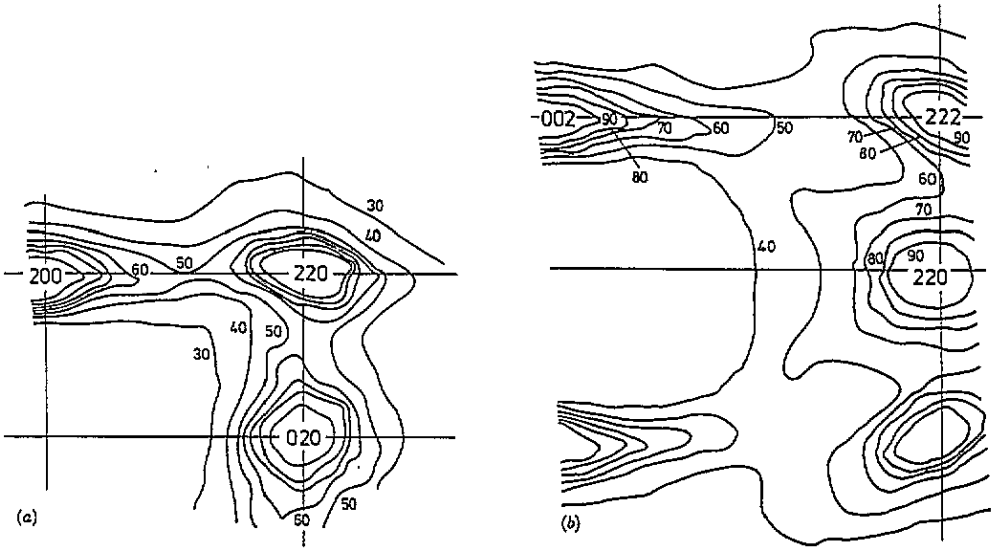

Figure 4. Diffuse x-ray scattering of NaOH observed (*a*) in the plane containing the 200, 020 and 220 Bragg peaks and (*b*) in the plane containing the 002, 220 and 222 Bragg peaks.

The strong diffuse scattering extending far into the regions between the Bragg reflections is interpreted as thermodiffuse scattering (TDS) mainly caused by the low-frequency acoustic modes, the intensity being inversely proportional to the frequencies squared (see, e.g., Wills and Pryor (1975)):

$$I \propto \sum_i \frac{(Q \cdot e_i)^2}{\Omega_i^2} \tag{9}$$

with $e_i = e_i(q)$ the polarization vectors of the mode of frequency Ω_i and wavevector q; Q is the scattering vector and $Q = G + q$, where G is a reciprocal-lattice vector.

Thus the analysis of the intensity gives an estimate of the frequencies and the elastic constants under the assumption that the optical excitations are of sufficiently high frequency that their contribution is negligible. This is true at least close to the zone centre where the frequencies of the acoustic modes go to zero.

Since there is less diffuse scattering on the lines connecting the origin with the Bragg reflections, the longitudinal dispersion must rise steeply and the corresponding elastic constants must be high. The branch polarized along the [001] direction can be observed near the 200 reflection. It is visible throughout the entire Brillouin zone. The branch polarized along the [110] direction can be observed around the 220 reflection. Since near the latter

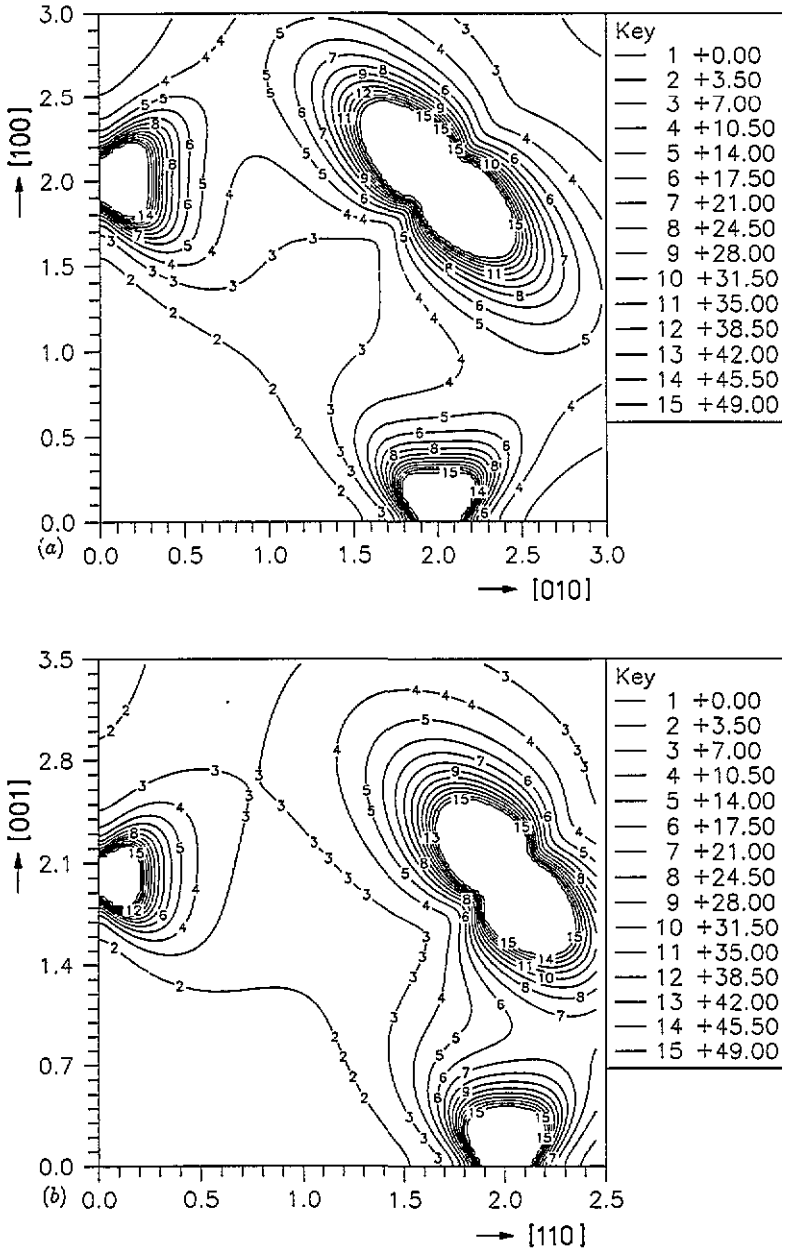

Figure 5. Diffuse x-ray scattering of NaOH calculated from (9) in the same planes as in figure 4.

the intensity is stronger, one can conclude that the elastic constant $(c_{11} - c_{12})/2$ is smaller than c_{44}.

In figure 5 the TDS computed from (5) with the elastic constants from the inelastic data discussed below is shown. The theoretical interpretation, namely the connection between this strong TDS and the OH reorientation dynamics, has been given in I and will be briefly repeated when discussing the unusual phonon behaviour.

5. Disorder scattering of D

A neutron scattering diagram of polycrystalline NaOD (Bleif 1978) shows a broad background which peaks between the reflections 200 and 220 which is not found in the monoclinic phase; it is attributed to scattering due to the disorder in the spatial distribution of D.

In order to determine the directional dependence, the diffuse scattering from a single crystal of NaOD was measured at the IN2 at the ILL, Grenoble, in different Q directions. The results for one of the elastic scans, corrected for incoherent and phonon contributions (for details see Kabs (1982)) are shown in figure 6(a).

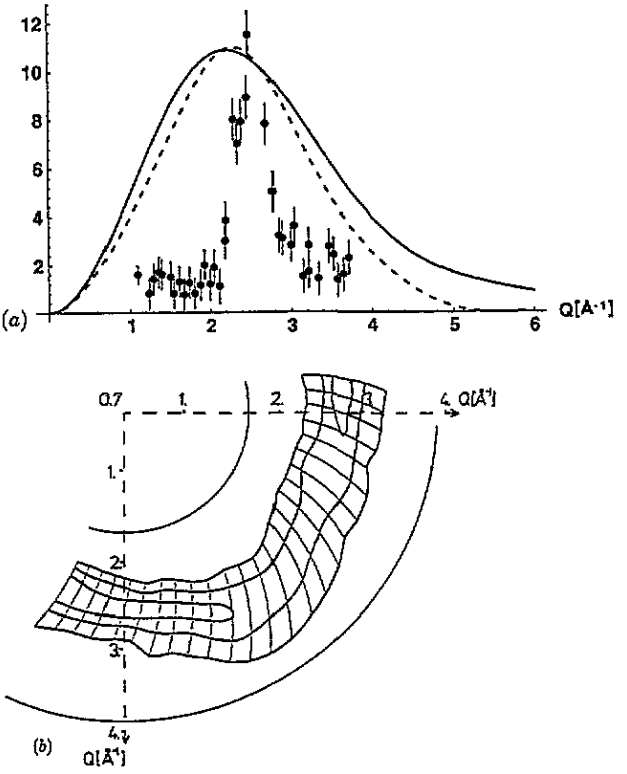

Figure 6. (a) Coherent elastic diffuse scattering of cubic NaOD along [1 0.1 0]; data from IN2 (ILL, Grenoble) integrated over ±2.5 meV (Kabs 1982). The lines are calculated as described in the text, the broken line referring to the correlation model. (b) Disorder scattering, with background subtracted, from single-crystal neutron diffraction in the $(h + 0.4\,h - 0.4\,l)$ plane with 250 counts per 40 min. The numbers on the axes refer to distances from the origin that is on the horizontal axes

$$\tilde{x} = \left|\frac{x^*}{\sqrt{2}}(1,1,0) + 0.4\frac{2\pi}{a}(1,-1,0)\right| = \sqrt{(x^*) + (0.7)^2}$$

is counted and on the vertical axis

$$\tilde{z} = \left|z^*(0,0,1) + 0.4\frac{2\pi}{a}(1,-1,0)\right| = \sqrt{(z^*)^2 + (0.7)^2}.$$

Therefore the axes start with 0.7 and the ticks are not equidistant.

In addition, scans were performed at a one-dimensional multicounter (HMI, Berlin) with an angular range of 80°. The crystal was rotated around the [110] axis in steps of 5° and the scattering was recorded in the angular range $2\theta = 33$–$113°$, using a wavelength of 2.4 Å.

In addition to the reciprocal-lattice plane (hhl) the plane $(h + 0.04\,h - 0.4\,l)$ was recorded in order to avoid the scattering from Bragg reflections; for this purpose the multicounter was lowered accordingly.

The single-crystal results confirm a diffuse halo around the origin in Q-space which is essentially spherical with a radius of about 2.5 $Å^{-1}$ superimposed on streaks of phonon scattering similar to the diffuse x-ray scattering. After subtraction of the latter and background correction the result is as shown in figure 6(b).

The disorder diffuse scattering (DDS) from an OH complex is given (up to a constant factor) by

$$I_{DDS} = \frac{1}{N}\sum_n I_n \qquad I_n = \left|\exp^{(iQ\cdot r_n)} - \frac{1}{N}\sum_m \exp^{(iQ\cdot r_m)}\right|^2 \tag{10}$$

where depending on the model the sites r_n can be the positions of a 'split-atom' model, say the corners and edges of a cube with oxygen in the centre, or the sites are taken distributed on a sphere around the oxygen. Detailed results are given in the appendix. The corner plus edges model leads to the full line in figure 6(b).

The narrowness of the experimental DDS peak, which is obvious in figure 6(a), might indicate correlations between the orientations of neighbouring OH groups. Therefore, in addition to the rather trivial (uncorrelated) disorder scattering above, also a two-dimensional (2D) 'avoidance correlation' model is described in the Appendix; it is based on the idea that two close H ions repel each other.

The narrowing effect on the diffuse halo from this calculation is much less than expected, (see figure 6(a), broken curve, and also figures A2(a) and A2(b)). Now on the one hand the narrowness may also be the result of subtracting too much background and too many quasi-elastic contributions, for which at the time of the experiments no theoretical interpretation was available, and on the other hand the model is probably too simple, especially in view of the probably large dipole moments†. It seems well worth reconsidering the details of disorder scattering again, both experimentally and theoretically.

6. Phonons in NaOD

In order to obtain more information on the dynamics of NaOD and KOD, the scattering was investigated using the three-axis spectrometers IN2 and IN8 a Grenoble. Constant-q scans (q referring to the length of the phonon wav performed around the 020 and 220 reflections with a wavevector of instrumental resolution was 0.23 THz. A few scans close to the 0? performed with 1.55 $Å^{-1}$; in this case the resolution was 0.05 THz a phonons from Bragg scattering down to a reduced wavevector of 0.0? same results have been obtained for NaOD and KOD. The essential been reported in I.

Figure 7 shows the dispersions extracted from the inelastic dat vertical bars indicating the broadening of the phonon groups. Th are relatively well defined. Their dispersion curves rise steeply; the q-values is limited by the energy transfer available. The transverse only for small wavelengths; they broaden and disappear near the zone. The dispersion of the modes polarized in the (100) direction

† As a defect in KBr, KCl and RbCl, OH^- is known to have a dipole moment of of CN with 0.3–0.5 Debyes (data from Lüty compiled in a table by Narayanamurti a

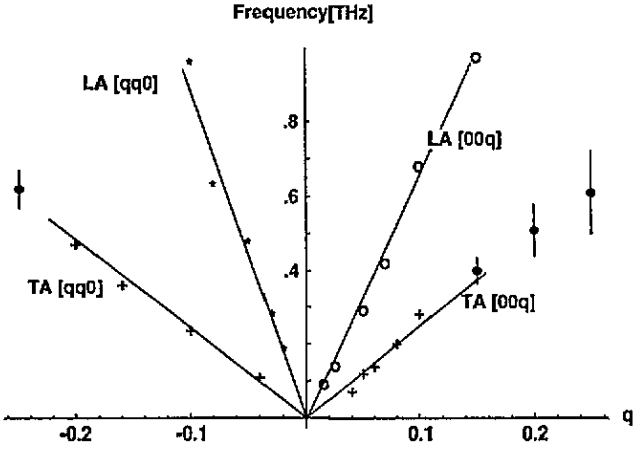

Figure 7. Experimentally determined dispersions for NaOD with slopes corresponding to $c'' = 1.6 \times 10^{10}$ dyn cm^{-2}, $c_{44} = 4.4 \times 10^{10}$ dyn cm^{-2}, $c_{11} = 23 \times 10^{10}$ dyn cm^{-2} and $c' = 25.2 \times 10^{10}$ dyn cm^{-2}; for definitions and polarizations see table 4.

that of modes polarized in the ⟨110⟩ direction, which is consistent with the diffuse x-ray scattering. Optical modes could not be detected within the accessible energy range up to 2 THz.

Figures 8, 9 and 10 show experimental results for the shear mode with elastic constant c_{44}, for the longitudinal mode c_{11} measured along the cubic edge $q \parallel [100]$ and for c'' measured along the face diagonal $q \parallel [110]$.

The phonon results resemble those of the cyanides KCN and NaCN with their dynamically disordered CN groups in the high-temperature structure; for a recent review and references see Höchli *et al* (1990). Here the unusual features are even stronger because the OH or OD groups flip faster due to the higher temperatures, around 550 K, assuming Arrhenius behaviour for the flip rates.

In addition, while the CN dumbbells have more definitely preferred high-symmetry
ons, the hydrogen has an almost spherical probability distribution around the oxygen
isturbance of all phonons is expected. As for the CN groups, for OH and OD the
lastic dipoles (called quadrupoles by some workers) will be used and the electric
neglected in the discussion of the acoustic mode behaviour. The theoretical
is not adequate for treating optical modes anyway.
ons can in principle probe whether the regular lattice motions are slower
pseudo-spins. When the latter are very fast, the neutrons of relatively
an average soft medium with well defined phonon peaks connected to
astic constants. At short wavelengths and high frequencies of the lattice
ns can appear almost static to the neutrons, giving rise to a Huang-
component, in addition to well defined phonon peaks connected to
s. At intermediate wavelengths the phonons appear overdamped.
n be observed for example for the c_{44} mode in $CsCuCl_3$ in the high-
af *et al* 1989, Graf and Förster 1995). The experimental dispersions
s indicate that, for the shear modes, mostly the 'softened mode' and
nes are observed; that is, to the neutrons of shear-wave velocity for
illouin zone the flipping dipoles never look quasi-static, the flip rate
$CsCuCl_3$ and the cyanides.

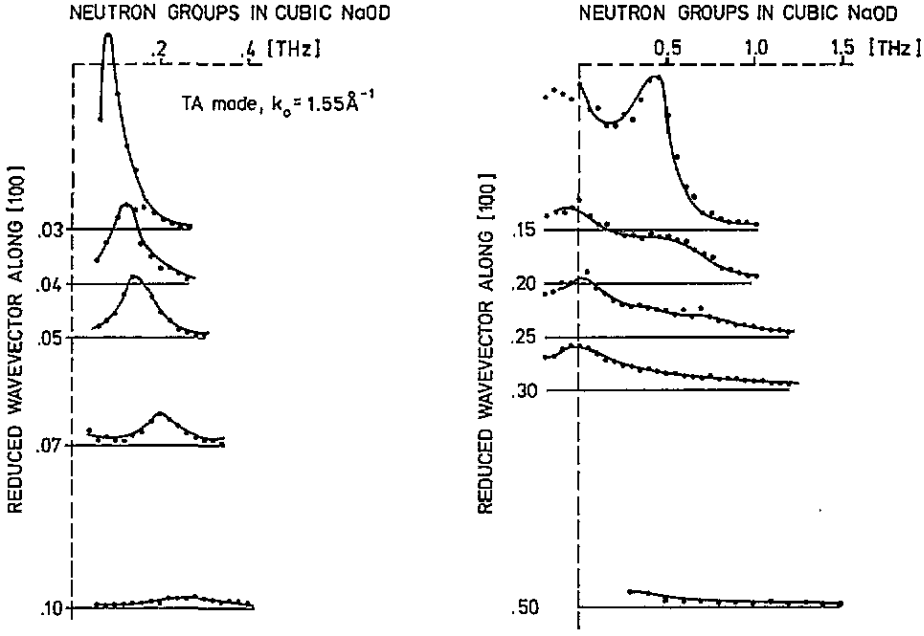

Figure 8. Original data for NaOD from inelastic neutron scattering: constant-q scans for the c_{44} shear mode for different q ranges. The q-values are indicated on the vertical axis. The lines are guides for the eye.

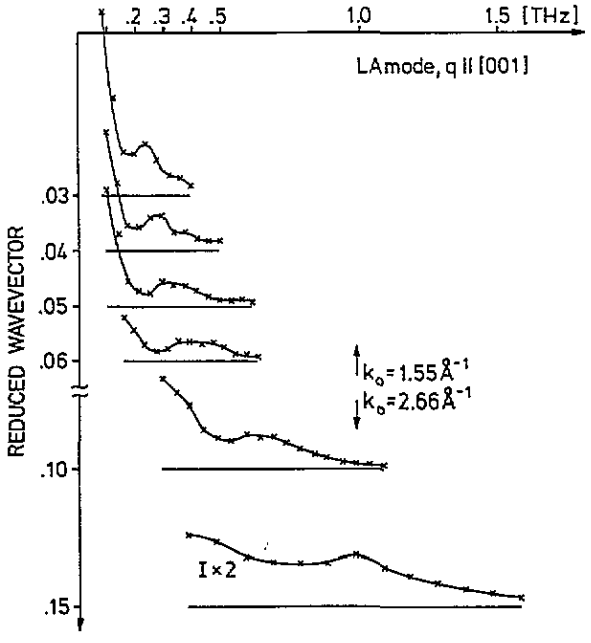

Figure 9. Original data for NaOD from inelastic neutron scattering: constant-q scans for the longitudinal c_{11} mode.

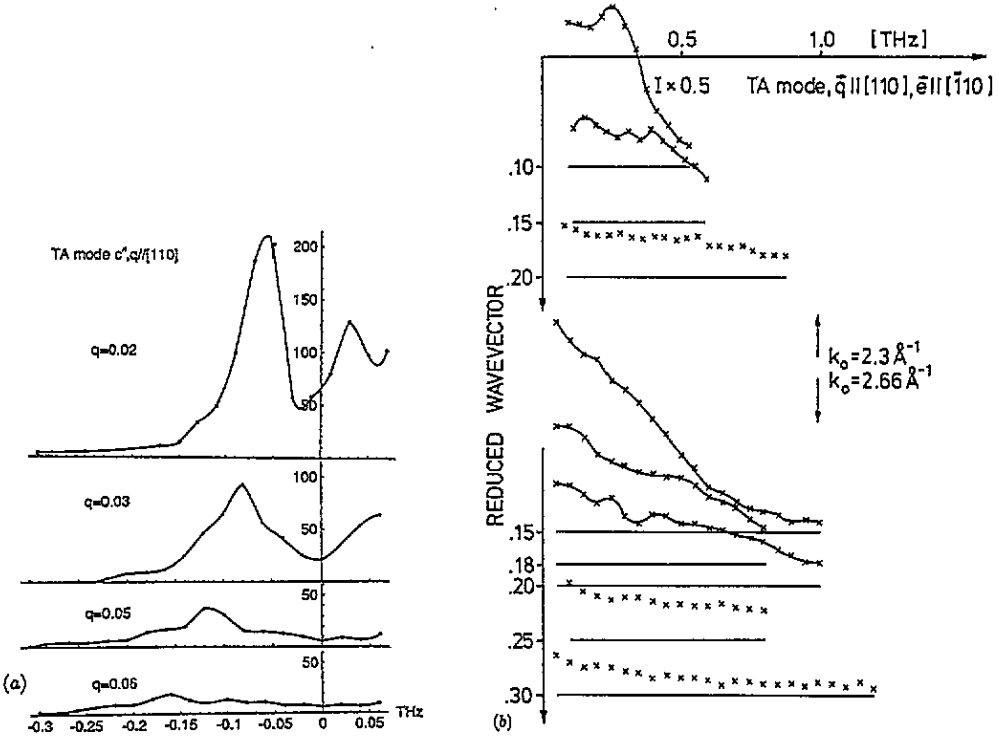

Figure 10. Original data for NaOD from inelastic neutron scattering: constant-q scans for the c'' shear mode for two different q ranges.

7. Elastic dipole model for the OH and OD groups and inelastic neutron scattering cross section

In the following a brief review of the theory developed in I is given. The system is taken as a cubic elastic medium containing elastic dipoles of different types depending on their direction coupled linearly to the distortions ε_{ij}:

$$H = \tfrac{1}{2}\sum_{ijkl}\lambda_{ijkl}\varepsilon_{ij}\varepsilon_{kl} + \sum_{ijrn} P^r_{ij}\varepsilon_{ij}c^r(\boldsymbol{R}_n) \tag{11}$$

where λ_{ijkl} are the elastic constants, P^r_{ij} are the components of the elastic dipole tensors and $c^r(\boldsymbol{R}_n)$ is either one or zero depending on whether dipole type r is in location $\boldsymbol{R}_n$ or not.

In an isotropic medium the components of an elastic dipole in direction $\boldsymbol{d}^r$ can be written as

$$P^r_{ij} = \alpha\{d^r_i d^r_j - (d^2/3)\delta_{ij}\} \tag{12}$$

where α is a strength factor and d is the length of $\boldsymbol{d}$, which is the same for all r. For the high-symmetry propagation directions where phonons have been measured, the OD groups of $\langle 111\rangle$, $\langle 110\rangle$ and $\langle 100\rangle$ directions are expected to couple; an example for a 'corner dipole' direction is $d_c = (1, 1, 1)$, for an edge dipole $d_e = \sqrt{3/2}(1, 1, 0)$, and for a dipole showing to a face centre $d_f = \sqrt{3}(1, 0, 0)$.

In an elastically anisotropic medium there will be different strength factors for diagonal and off-diagonal dipole tensor elements, proportional to the shear constants c_{44} and c'',

from the response of the medium to the elastic dipole orientations; for details see I. This complication is not very important for the following discussion.

After expanding (9) in normal acoustic modes and Fourier transformation the interaction term takes the form

$$H_{dd} = \sum_{qrj} \mathrm{i}(\mathbf{P}^r \boldsymbol{q} \cdot \boldsymbol{e}_j) A_j(q) c^r(-q) \tag{13}$$

where $\boldsymbol{e}_j$ is the normalized polarization vector of a mode $\omega_j(\boldsymbol{q})$ and a wavevector $\boldsymbol{q}$ and $A_j(q)$ is the phonon amplitude or normal coordinate, $c^r(q)$ is the Fourier transform of the concentration fluctuation $c^r(\boldsymbol{R}_n) - c$, with $c = 1/r_0$, with r_0 the number of dipoles of a certain type. The elastic dipoles play the role of pseudo-spins, their explicit form entering the spin–phonon interaction and the spin vector given by the concentration fluctuation.

After adding the entropy and diagonalizing the free energy with respect to the normal coordinates, the effective phonon energy becomes

$$H_{phon} = \tfrac{1}{2} \sum_{qj} \Omega_j^2(q) Q_j Q_j^* \tag{14}$$

with

$$\begin{aligned} \Omega_j^2(q) &= \omega_j^2(q) - \frac{1}{r_0} \sum_r \frac{(\mathbf{P}^r \boldsymbol{q} \cdot \boldsymbol{e}_j)^2}{kT} \\ &\equiv \omega_j^2(q) - \tfrac{1}{8} h_j^2(d_c) - \tfrac{1}{12} h_j^2(d_e) - \tfrac{1}{6} h_j^2(d_f) \end{aligned} \tag{15}$$

where for example

$$h_j^2(d_e) = \sum_r \frac{(\mathbf{P}^r \boldsymbol{q} \cdot \boldsymbol{e}_j)^2}{kT} \tag{16}$$

refers to the elastic dipoles along the cubic body diagonals. The $\omega_j(\boldsymbol{q})$ can be regarded as the modes of a reference system without orientational degrees of freedom. They are also the 'hard' modes in the 'slow dipole' regime described above.

From (15), one sees that all acoustic modes, transverse and longitudinal, undergo softening. Since the softening contribution is of the same order of magnitude for all modes, the effect is more dramatic for the transverse modes because of their smaller elastic constants. The softening contributions for the different modes are listed in table 4. One finds for example that, if the hydrogen were mostly localized in the corners of a cube around oxygen, then the shear mode with $c'' = (c_{11} - c_{12})/2$ would not soften at all, contrary to observations. When the hydrogen is on the edges of this cube, all modes are disturbed, but c'' only half as much as c_{44}.

The scattered neutron intensity is proportional to the inelastic scattering cross section

$$\frac{\mathrm{d}^2\sigma}{\mathrm{d}\omega\,\mathrm{d}\Omega} = \bar{b}^2 \sum_i (\boldsymbol{Q} \cdot \boldsymbol{e}_i(q))(\boldsymbol{Q} \cdot \boldsymbol{e}_i(q)) \langle A_i(q) A_i(q) \rangle_\omega \tag{17}$$

where the sum is over the three acoustic modes for each propagation vector $\boldsymbol{q}$ with $\boldsymbol{Q} = \boldsymbol{K} + \boldsymbol{q}$, where $\boldsymbol{K}$ is the Bragg point. The scattering length $\bar{b}$ contains the structure factor and the DW factor. By an appropriate choice of $\boldsymbol{K}$, one selects the type of wave that one wishes to study. Here the phonons along a cubic edge $\boldsymbol{q} = (q, 0, 0)$ and a face diagonal $\boldsymbol{q} = (1, 1, 0)q/\sqrt{2}$ have been investigated near the Bragg reflections 020 and 220.

Table 4. Acoustic modes in the cubic system and softening contributions to the elastic constants from face centre, corner- and edge-oriented elastic dipoles.

Wavevector	Polarization	Elastic constant	$h_i^2(d_f)/6$	$h_i^2(d_c)/8$	$h_i^2(d_e)/12$
$q=(q_x,0,0)$	$e_1=(1,0,0)$LA	c_{11}	$2\alpha^2q_x^2$	0	$\frac{1}{2}\alpha^2q_x^2$
	$e_2=(0,1,0)$, $e_3=(0,0,1)$ TA	c_{44}	0	$\alpha^2q_x^2$	$\frac{3}{4}\alpha^2q_x^2$
$q=(q/\sqrt{2})(1,1,0)$	$e_1=(1/\sqrt{2})(1,1,0)$LA	$c'=\frac{1}{2}(c_{11}+c_{12})+c_{44}$	$\frac{1}{2}\alpha^2q^2$	α^2q^2	$\frac{7}{8}\alpha^2q^2$
	$e_2=(1/\sqrt{2})(1,-1,0)$TA	$c''=\frac{1}{2}(c_{11}-c_{12})$	$\frac{3}{2}\alpha^2q^2$	0	$\frac{3}{8}\alpha^2q^2$
	$e_3=(0,0,1)$TA	c_{44}	0	α^2q^2	$\frac{3}{4}\alpha^2q^2$
$q=(q/\sqrt{3})(1,1,1)$	$e_1=(1/\sqrt{3})(1,1,1)$LA	$\frac{1}{3}(c_{11}+2c_{12}+4c_{44})$	0	$\frac{4}{3}\alpha^2q^2$	α^2q^2
	$e_2=(1/\sqrt{6})(-2,1,1)$, $e_3=(1/\sqrt{2})(0,-1,1)$ TA	$\frac{1}{3}(c_{11}-c_{12}+c_{44})$	α^2q^2	$\frac{1}{3}\alpha^2q^2$	$\frac{1}{2}\alpha^2q^2$

The phonon correlation function to be used, derived in I, is the generalization of that developed by Yamada *et al* (1974) for the softening of *one* acoustic mode ω_0 of amplitude A due to pseudo-spin–phonon coupling denoted by h:

$$\langle AA\rangle_\omega = \frac{kT}{\pi\gamma}\frac{h^2/kT}{(\omega^2-\omega_0^2+h^2/kT)^2+(\omega^2/\gamma^2)(\omega^2-\omega_0^2)^2}. \tag{18}$$

γ describes the relaxation process of the isolated pseudo-spin and γ^{-1} is the relaxation time of the flipping motion. Here and in the following, the frequencies are taken to be of the form

$$\omega_0=\sqrt{\frac{c}{\rho}}\frac{2\pi}{a}q \tag{19}$$

with $q=0\ldots\pm0.5$ in the Brillouin zone, $a=5.1$ Å is the lattice constant and $\rho=2$ g cm^{-3} is the density of NaOD; c is the (hard) elastic constant. When all modes soften, the correlation function to be used for ω_i, say $i=1$, involves also the other two modes with $i=2,3$:

$$\langle A_1A_1\rangle_\omega=\frac{kT}{\pi\gamma}\frac{h_1^2}{kT}(\omega^2-\omega_2^2)^2(\omega^2-\omega_3^2)^2\Big/\left(\prod_i\left(\frac{\omega^2-\omega_i^2+h_i^2}{kT}\right)^2+\frac{\omega^2}{\gamma^2}\prod_i(\omega^2-\omega_i^2)^2\right). \tag{20}$$

The products in the denominator are over the three eigenmodes for each propagation direction q. If only one mode softens, that is $h_2^2=h_3^2=0$, (20) reduces to (18). Analytically this form is satisfactory in the sense that it describes important limits correctly; the thermodiffuse x-ray scattering (9) is obtained by integration of (20) with respect to ω, and one finds the correct Huang limit for quasi-elastic scattering, i.e. for $\omega\to0$ and small flip rates γ (quasi-static elastic dipoles); for details see I.

The mixing effects to be discussed below are new; overdamping of one phonon mode can be visible in the phonon groups of another mode. In principle it should be possible to extract seven parameters for the cubic system, namely the three hard elastic constants, the three softened elastic constants and the flip rate, by measuring in the three main symmetry directions, i.e. edge, face and body diagonals. To check the consistency, one should measure c_{44} also from the degenerate mode propagating along the cubic edge as well as from the non-degenerate mode along the face diagonal; different lineshape and mixing effects are expected.

The available results are not complete in this sense and are not sufficient to fix unambiguously all unknown parameters. Note that there has been a considerably time lapse between the experiments (1979) and the development of the theory.

One can start a semiquantitative evaluation of (20) by taking the values of the elastic constants from the experimental dispersions for the softened constants and $\gamma = 0.45$ THz from the work of Smit *et al* (1979). Comparing experimental and calculated constant-q scans, one then finds estimates for the hard elastic constants that have to be consistent with each other with respect to the elastic dipole contributions from table 4.

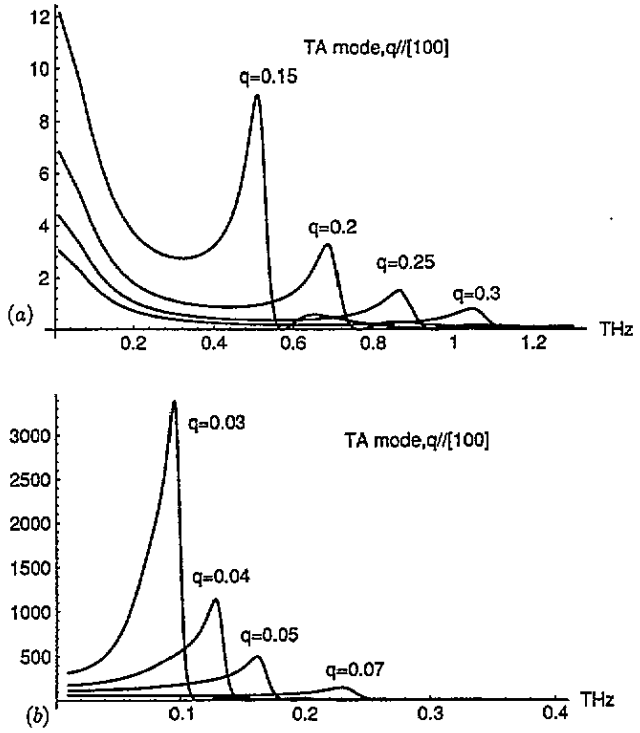

Figure 11. Simulation of c_{44} phonon groups from (20) to be compared to figure 8, with $c_{44} = 4.4 \times 10^{10}$ dyn cm^{-2} (7.6×10^{10} dyn cm^{-2}) and $c_{11} = 23 \times 10^{10}$ dyn cm^{-2} (33×10^{10} dyn cm^{-2}), where the hard values are in parentheses; $\gamma = 0.8$ THz.

The shear mode with c_{44} measured as degenerate transverse mode along $q = (q, 0, 0)$ (figure 8) is straightforward to interpret because the accompanying c_{11} mode interferes little, c_{11} being much larger than c_{44}; this means that (18) and (20) give qualitatively the same picture for the c_{44} phonon groups, as below in figure 12. One clearly observes the transition from a well defined softened mode (figures 8(a) and 11(a)) to the regime of overdamping (figures 8(b) and 11(b)). From this measurement, one can determine c_{44}, but not so easily c_{11}. This is done by comparing the c_{11} results (figures 9 and 12). The peaks correspond to the softened c_{11} mode. This figure would look quite different with (18); the intensity at small energy transfers comes from the admixture of c_{44}.

So, from these two measurements, reasonable values of the hard and soft values of c_{11} and c_{44} can be determined. The c_{44} modes are not very sensitive to changes in γ; values between 0.45 and 0.9 THz yield acceptable phonon group simulations. The c_{11} modes are even less sensitive to these γ variations. We return to this point below.

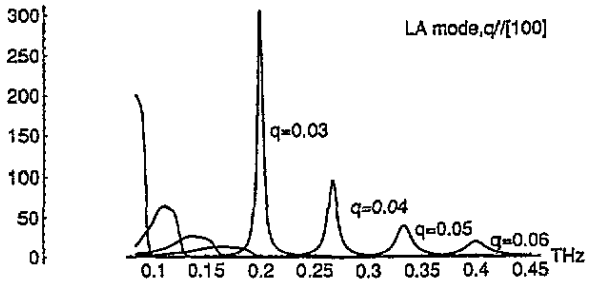

Figure 12. Simulation of c_{11} phonon groups from (20) to be compared to figure 9; the parameters are as for figure 11, but $\gamma = 2$ THz.

The measurements with $q = (1, 1, 0)q/\sqrt{2}$ involve the three modes related to $c' = (c_{11} + c_{12})/2 + c_{44}$, c_{44} and c''. The c_{44} parameters can now be taken as known; note that we have the mixture of two shear modes expected to soften in the same q range.

From figure 10, one sees that the c'' phonon peaks are well defined only up to $q = 0.06$ and then merge into the background. Surprisingly neither (18) nor (20) can reproduce this observation unless one considerably increases the value of γ.

We propose that the reason for the faster flips is the small density probability of the proton for the face centres of the cube around the oxygen found from the structure determination: from table 4, one sees that the face centre dipoles give the dominant contribution to the softening of the c'' shear mode. The same holds for the longitudinal c_{11} mode but, as we noted before, the harder modes are not very sensitive to the flip rate; the qualitative picture, such as figure 12 stays the same. Since the occupation probability of the face centres is only 20% of that of the corners, we used $\gamma = 2$ THz for the plot in figure 13, more for demonstration purposes than to offer this value as really definite; the pictures would look quite similar for, say, $\gamma = 1.5$ THz. The choice of γ also affects the width and strength of the central contribution (quasi-elastic part) which, however close to the Bragg reflection, is not easy to identify. There is also correlation between the hard elastic constants and flip rate parameters.

The fine structure in figure 13(a) is due to mixing with the c_{44} mode and experimentally expected to be hidden within the resolution. The theory reproduces the observed behaviour that the c'' modes even for small q become overdamped so that beyond 0.1 (figure 13(b)) no hint of this mode can be identified. The small remaining humps come from the c_{44} mode.

8. Summary

Details on the structure and dynamics of the alkali hydroxides in their high-temperature cubic phase are reported and interpreted.

From single-crystal neutron diffraction, very large DW factors and a nearly spherical probability density for the hydrogen around the oxygen result. Interesting details are the fact that the DW factor is largest for the alkali ion, pointing to evasive motions due to the reorientations of the OH group which probably causes strong disturbance of the acoustic modes. Further the H density is much smaller in the [100] direction than in the [111] or [110] direction. Diffuse x-ray scattering and neutron scattering from single crystals have also been measured. With neutrons the disorder of the hydrogen is seen as a broad halo around the centre in Q-space. The fact that this halo is narrower than expected points to correlations between the OH reorientations. The broad thermodiffuse x-ray scattering is in

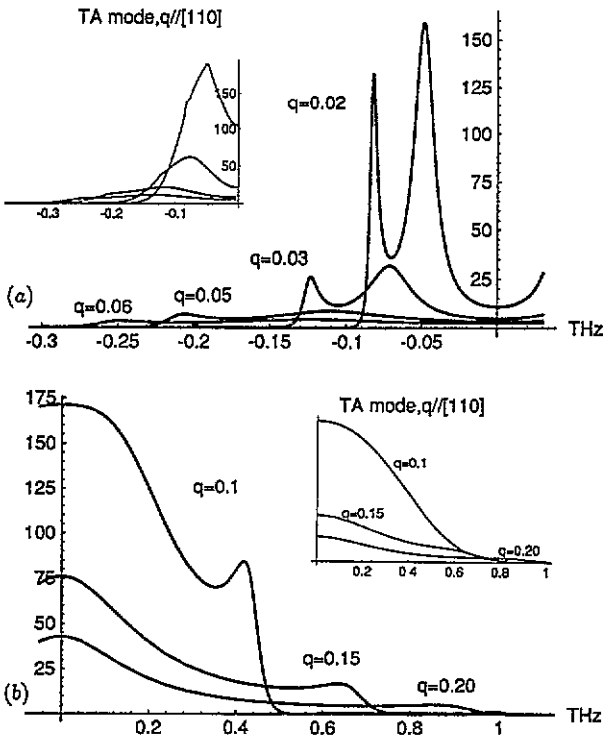

Figure 13. (*a*) Simulation of c'' phonon groups from (20) for very small q, to be compared to figure 10(*a*), the double peaks come from mixing with the c_{44} mode but will merge into one by resolution effects; see inset where a resolution of 0.02 THz has been applied. (*b*) Evaluation of (20) for the c'' mode for larger q; inset has a resolution of 0.06 THz. The parameters used are $c'' = 1.6 \times 10^{10}$ dyn cm^{-2} (9.8×10^{10} dyn cm^{-2}), $c_{44} = 4.4 \times 10^{10}$ dyn cm^{-2} (7.6×10^{10} dyn cm^{-2}) and $c' = 25.8 \times 10^{10}$ dyn cm^{-2} (30.8×10^{10} dyn cm^{-2}) for soft (hard) elastic constants and $\gamma = 2$ THz.

full agreement with the softening of the shear modes found from the inelastic data, yielding small values of the elastic constants c_{44} and $c'' = (c_{11} - c_{12})/2$.

The dynamic features that can be deduced from the structure information are contained in the theoretical description of the inelastic neutron data. The OH groups are treated as elastic dipoles with the dynamics of a relaxator. In our interpretation the anisotropic H^+ density distribution leads to anisotropic relaxational behaviour of these dipoles. The constant-q scans are semiquantitatively simulated; they reflect the competition between the fast reorientations of the OH groups and the regular lattice motions. The relatively slow shear modes are strongly affected; the (softened) modes are observable only up to about 0.1 of the Brillouin zone and appear overdamped beyond that. The longitudinal modes are also influenced by the OH dynamics but stay well defined, and could in principle be followed throughout the Brillouin zone, the then relatively slow OH reorientations contributing a central component. In addition, mixing effects from different modes can be identified. In fact, the softening effects are expected to be temperature dependent, the elastic constants being of the form $c = c_0(1 - a/T)$; due to its wider cubic phase, only KOD would be a candidate for such an investigation.

Appendix A. Disorder diffuse scattering

Disorder scattering is caused by the distribution of possibly H^+ positions around the oxygen partner and produces an intensity halo, roughly spherical, around the origin in reciprocal space with a radius inversely proportional to the average OH distance. Finer details of the intensity distribution give clues to details of the non-sphericity of the H^+ distribution in real space and to correlations between H^+ motions of the neighbouring groups.

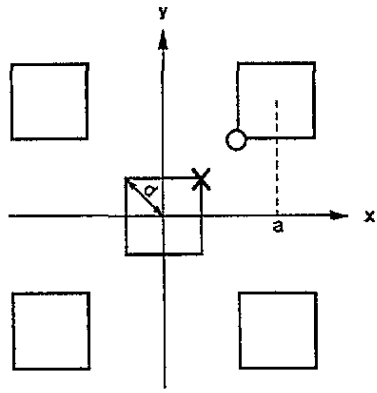

Figure A1. 2D model for correlated jumps for a simple split-atom model. The protons can sit only on corners and not simultaneously on nearest-neighbour corners.

Without correlations the DDS for one OH complex is calculated as

$$I_{DDS} = \langle (f_n - \langle f_n \rangle)^2 \rangle = \langle f_n^2 \rangle - \langle f_n \rangle^2 \qquad \text{with } f_n = \exp(\mathrm{i}\boldsymbol{Q} \cdot \boldsymbol{r}_n) \tag{A1}$$

and averaging over the available sites means that $\langle \cdots \rangle = (1/N) \sum_n \cdots$ so that

$$I_{DDS} = \frac{1}{N} \sum_n \left| f_n - \frac{1}{N} \sum_m f_m \right|^2 = \frac{1}{N} \sum_n |f_n|^2 - \left| \frac{1}{N} \sum_m f_m \right|^2. \tag{A2}$$

Depending on the model, the sites $\boldsymbol{r}_n$ are the corners of a cube (model used by Smit *et al* (1979)) or the 20 positions of the corners plus edge middles, or the sites could be assumed to be distributed continuously over a sphere. For these examples, one simply obtains for the DDS intensity

$$I_{corner} = 1 - f_c^2 \qquad \text{(corner)} \tag{A2a}$$

$$I_{e\&c} = 1 - \left(\frac{8 f_c + 12 f_e}{20} \right)^2 \qquad \text{(edge and corner)} \tag{A2b}$$

with

$$f_c = \cos(Q_x d) \cos(Q_y d) \cos(Q_z d)$$

$$f_e = (\cos(Q_x e) \cos(Q_y e) + \cos(Q_x e) \cos(Q_z e) + \cos(Q_z e) \cos(Q_y e))/3$$

$$d = R_H/\sqrt{3}$$

$$e = R_H/\sqrt{2}$$

and for the spherical distribution

$$I_{sphere} = 1 - \left(\frac{\sin(Q d_{OH})}{Q d_{OH}} \right)^2 \qquad Q = |\boldsymbol{Q}| \tag{A2c}$$

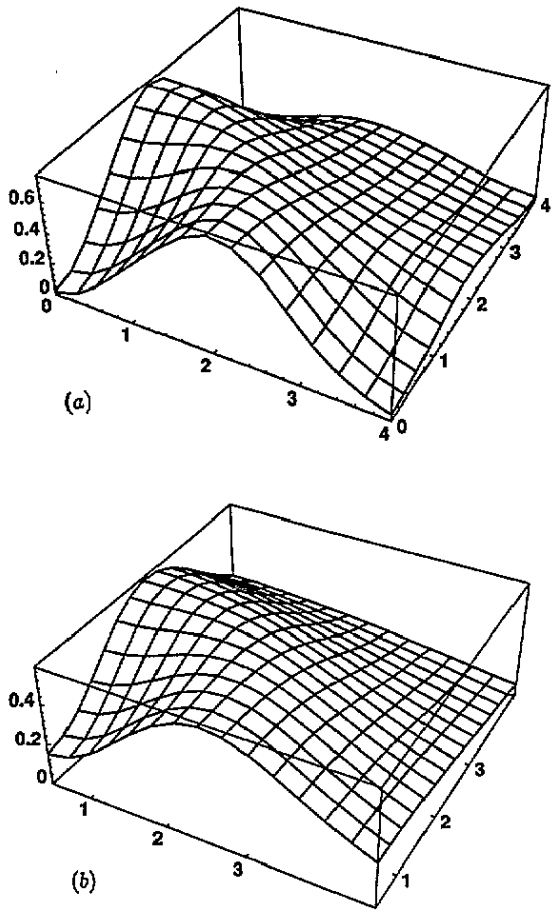

Figure A2. (*a*) Distribution of DDS in the (001) plane for the 2D correlation model. (*b*) DDS for the split-atom model with positrons on corners and edges; the geometry is as in figure 6(*b*). The intensity on the vertical axis is as obtained from equations (A2) and (A3).

with the OH distance R_H taken as 1 Å for simplicity.

These expressions for the DDS have to be multiplied by the appropriate DW factor. The 'split-atom' model should be more realistic since it still contains features of cubic symmetry as implied by the results of the Press–Hüller ansatz above. The above expressions, e.g. with $\exp(-0.09Q^2)$ as the DW factor for NaOD, yield rather broad maxima between 2 and 3 $Å^{-1}$; therefore the diffuse halo passes through the 002 Bragg reflection ($4\pi/a = 2.46$ Å) and there is some uncertainty to sorting out the DDS from TDS. Still it seemed that the observed halo was narrower than expected from (A2); this could be caused by correlations between the motions of H^+ ions of different OH groups. We therefore make an attempt to include them. For this purpose the split-atom model is the most convenient. We use the simplest possible 2D model which can describe the fact that next-neighbour H^+ ions repel, whether it is by the tendency of steric avoidance or by the electric dipole 'head-to-tail' ordering tendency. As sketched in figure A1, only corner positions of the 2D FCC lattice are considered; the centre oxygen is not shown. The nearest-neighbour positions X and O, will not be occupied simultaneously. Consider first these two squares: if X is occupied, there are three possible next nearest positions for the other H^+ and similarly if O is occupied; these six arrangements

each have an occupation probability of 3/4. Then there are nine pair states where neither X nor O is occupied, each with a weight of 9/16. Later by imposing cubic symmetry all such arrangements of the unit cell can be collected.

For this 'molecular' model a generalized form of averaging in (A1) has to be used:

$$I_{DDS} = \frac{1}{N}\left(\sum_n p_n|F_n|^2 - \left|\frac{1}{N}\sum_m p_m F_m\right|^2\right). \tag{A4}$$

The pair structure factors are typically of the form $F = \exp(\mathrm{i}\boldsymbol{Q}\cdot\boldsymbol{r}_n^1) + \exp(\mathrm{i}\boldsymbol{Q}\cdot\boldsymbol{r}_n^2)$, where $\boldsymbol{r}_n^1$ and $\boldsymbol{r}_n^2$ are the corner positions of the two squares considered and can be expressed by the lattice constant a and OH distance d (see figure A1). The weights for nearest-neighbour pairs are $p_m^{(nn)} = 3p/4$ and for the others $p_m^{(nnn)} = 9p/16$; they are the same for all m. The normalization factor p is determined by the obvious condition that

$$\left(6\tfrac{3}{4} + 9\tfrac{9}{16}\right) p = 1$$

i.e. is $p^{(nn)} = 2/51$ and $p^{(nnn)} = 1/34$.

The calculation of (A3) is straightforward but gives a long and clumsy expression which is to be multiplied by the DW factor and put into a computer to obtain for example the intensity distribution in the $Q_z = 0$ plane, shown in figure A2(a). Compared to that for the uncorrelated model in figure A2(b) the difference is slight. Experimentally a distinction cannot be expected, realizing that our model even exaggerates the correlation effect compared to the real 3D situation where, because of the nearly spherical distribution, the H^+ ions have an even better chance to avoid 'seeing' next neighbours.

References

Bastow T J, Elcombe M M and Howard C J 1986a *Solid State Commun.* **57** 339–41
——1986 *Solid State Commun.* **59** 257–9
Bleif H J 1978 *Thesis* Universität Tübingen
——unpublished
Bleif H J and Dachs H 1982 *Acta Crystallogr.* A **38** 470–6
El'kin B S 1990 *Solid State Ion.* **37** 139–48
Graf H A and Forster U 1995 to be published
Graf H A, Shirane G, Schotte U, Dachs H, Pyka N and Iizumi M 1989 *J. Phys.: Condens. Matter* **1** 3743–63
Höchli U T, Knorr K and Loidl A 1990 *Adv. Phys.* **39** 405–615
Ibers J A, Kumamoto J and Snyder R G 1969 *J. Chem. Phys.* **33** 1164–70
Kabs M 1982 *Thesis* Technische Universität Berlin
Mach B, Jacobs H and Schaefer W 1987 Z. *Anorg. Chem.* **553** 187–95
Maurice M 1968 *Rev. Chim. Mineral.* **5** 89–94
Narayanamurti V and Pohl R O 1970 *Rev. Mod. Phys.* **42** 201–35
Press W 1973 *Acta. Crystallogr.* A **29** 257–63
Press W and Hüller A 1973 *Acta Crystallogr.* A **29** 252–6
Press W, Grimm H and Hüller A 1979 *Acta Crystallogr.* A **35** 881–5
Schotte U, Graf H A and Dachs H 1989 *J. Phys.: Condens. Matter* **1** 3765–87
Schotte U, Kabs, M, Dachs H and Schotte K D 1992 *J. Phys.: Condens. Matter* **4** 9283–98
Schotte U, Schotte K D, Bleif H J and Papoular R 1995 *Acta Crystallogr.* A at press
Seymor R S and Pryor A W 1970 *Acta Crystallogr.* B **26** 1487–892
Sherwood J N 1979 *The Plastically Crystalline State* (New York: Wiley)
Smit J G, Dachs H and Lechner R E 1979 *Solid State Commun.* **29** 219–23
Stull D R, Hildenbrand D L, Oetting F L and Sinke G C 1970 *J. Chem. Eng. Data* **15** 219–23
White M A and Moore S A 1986 *J. Chem. Phys.* **85** 4629–31
Willis B T M and Pryor A W 1975 *Thermal Vibrations in Crystallography* (Cambridge: Cambridge University Press)
Yamada Y, Takatera H and Huber D L 1974 *J. Phys. Soc. Japan* **36** 641–8